



THE UNIVERSITY *of* EDINBURGH

Edinburgh Research Explorer

Identification of Phase Transitions and Metastability in Dynamically Compressed Antimony using Ultra-Fast X-Ray Diraction

Citation for published version:

Coleman, A, Gorman, MG, Briggs, R, McWilliams, R, McGonegle, D, Bolme, CA, Gleason, AE, Fratanduono, DE, Smith, RF, Galtier, E, Lee, HJ, Nagler, B, Granados, E, Collins, GW, Eggert, JH, Wark, JS & McMahon, M 2019, 'Identification of Phase Transitions and Metastability in Dynamically Compressed Antimony using Ultra-Fast X-Ray Diraction', *Physical Review Letters*.
<https://doi.org/10.1103/PhysRevLett.122.255704>

Digital Object Identifier (DOI):

[10.1103/PhysRevLett.122.255704](https://doi.org/10.1103/PhysRevLett.122.255704)

Link:

[Link to publication record in Edinburgh Research Explorer](#)

Document Version:

Peer reviewed version

Published In:

Physical Review Letters

General rights

Copyright for the publications made accessible via the Edinburgh Research Explorer is retained by the author(s) and / or other copyright owners and it is a condition of accessing these publications that users recognise and abide by the legal requirements associated with these rights.

Take down policy

The University of Edinburgh has made every reasonable effort to ensure that Edinburgh Research Explorer content complies with UK legislation. If you believe that the public display of this file breaches copyright please contact openaccess@ed.ac.uk providing details, and we will remove access to the work immediately and investigate your claim.



Identification of Phase Transitions and Metastability in Dynamically-Compressed Antimony using Ultra-Fast X-Ray Diffraction

A. L. Coleman,^{1,2} M. G. Gorman,^{1,2} R. Briggs,^{1,2} R. S. McWilliams,¹ D. McGonegle,³ C. A. Bolme,⁴ A. E. Gleason,^{4,5} D. E. Fratanduono,² R. F. Smith,² E. Galtier,⁶ H. J. Lee,⁶ B. Nagler,⁶ E. Granados,⁶ G. W. Collins,⁷ J. H. Eggert,² J. S. Wark,³ and M. I. McMahon¹

¹*SUPA, School of Physics & Astronomy, and Centre for Science at Extreme Conditions, The University of Edinburgh, Edinburgh, EH9 3FD, UK*

²*Lawrence Livermore National Laboratory, 7000 East Avenue, Livermore CA 94500, USA*

³*Department of Physics, Clarendon Laboratory, Parks Road, University of Oxford, Oxford, OX1 3PU, UK*

⁴*Shock and Detonation Physics, Los Alamos National Laboratory, PO Box 1663, Los Alamos, New Mexico 87545, USA*

⁵*Department of Geological and Environmental Sciences, Stanford University, Stanford, California 94305, USA*

⁶*Linac Coherent Light Source, SLAC National Accelerator Laboratory, Menlo Park, CA 94025*

⁷*Department of Mechanical Engineering, University of Rochester, 235 Hopeman Building, PO Box 270132, Rochester, NY 12647, USA*

(Dated: May 21, 2019)

Ultrafast x-ray diffraction at the LCLS x-ray free electron laser has been used to resolve the structural behaviour of antimony under shock compression to 59 GPa. Antimony is seen to transform to the incommensurate, host-guest phase, Sb-II, at ~ 11 GPa, which forms on nanosecond timescales with ordered guest-atom chains. The high-pressure bcc phase, Sb-III, is observed above ~ 15 GPa, some 8 GPa lower than in static compression studies, and mixed Sb-III/liquid diffraction are obtained between 38 and 59 GPa. An additional phase which does not exist under static compression, Sb-I', is also observed between 8 and 12 GPa, beyond the normal stability field of Sb-I, and resembles Sb-I with a resolved Peierls distortion. The incommensurate Sb-II high-pressure phase can be recovered metastably on release to ambient pressure, where it is stable for more than 10 ns.

PACS numbers: 64.70.D- 62.50.-P 81.30.Bx 62.50.Ef

Under dynamic compression, antimony is a classic phase-transforming element [1]. Of particular note has been the anomalously-long transition time of 2-3 μ s determined for the shock-induced phase transition at 8.8 GPa [1–3]. Shock compression studies of antimony to date have typically used explosively-generated shock waves, and the existence of phase transitions has been inferred from measurements of the shock wave profiles [1–5], where complex, multiple wave structures greatly complicated the analysis.

The room-temperature phase transition sequence in antimony under static compression has been determined in detail using x-ray diffraction. Antimony crystallises in the A7 structure (Sb-I, space group $R\bar{3}m$, atom on $(0,0,u)$ with $u=0.234$) at ambient conditions, which is a Peierls-distorted simple-cubic (sc) structure. On compression, the c/a ratio of Sb-I decreases as the distortion relaxes and a sc phase (where $c/a = \sqrt{6}$ and $u=\frac{1}{4}$) is approached. While early studies reported a transition to the sc phase (hereafter Sb-I') at ~ 7 GPa [6–8], later diffraction studies [9–11] showed this phase is not obtained, but rather that Sb-I transforms to an incommensurate host-guest (HG) structure at ~ 8 GPa [11]. This phase, Sb-II, then persists up to 28.8 GPa at 300 K, where it then transforms to the body-centred cubic (bcc) structure of Sb-III. Recent diffraction studies have observed a modest temperature effect on the transformation pressures [13].

The absence of a suitably bright, short-pulsed x-ray source has long prevented a similar level of detail being obtained in shock compressed samples. However, x-ray free electron lasers (XFELs) now provide 50 fs pulses of monochromatic x-rays that are ideal for structural studies of dynamically-compressed matter. Here we report a study utilising laser compression and x-ray pulses from the Linac Coherent Light Source (LCLS) XFEL to study the structural behavior of shock-compressed Sb to 59 GPa. We find that in contrast to static-compression studies, Sb-I' is obtained via a fast (nanosecond or less) phase transition from Sb-I at 7.9 GPa. Diffraction profiles from Sb-I' differ markedly from those from Sb-I, and they can be fitted equally well by either a sc structure with distorted Debye-Scherrer (D-S) rings arising from sample strength, or a rhombohedral structure with $c/a \leq \sqrt{6}$. Shock-compression to higher pressures results in further transitions - to the incommensurate Sb-II phase at 11.3 GPa, to the bcc Sb-III phase at 14.6 GPa, and to the liquid phase above 37.6 GPa. All of these transitions take place on nanosecond timescales or less, as seen in Bi and Sc [14, 15]. On pressure release from the high-pressure phases, we find, for the first time, that the incommensurate phase can be recovered metastably to ambient pressures, where it has a lifetime of more than 10 ns.

Experiments were performed at the Matter in Extreme Conditions (MEC) end station of the LCLS [16].

Ablation-driven shock waves were generated using a Nd:glass optical laser (527 nm, 20 ns, quasi-flat-topped pulses [17]) and were used to compress the target package which consisted of a 50 μm thick polyimide ablator and a 10 μm thick, deposited Sb layer. Additional data were collected using targets with a 500 μm thick LiF window affixed to their rear [15]. The monochromatic pulses provided by the LCLS ($\lambda = 1.240\text{\AA}$) were focused to a 50 μm diameter spot, and then centered on the variable diameter (150 - 500 μm) focal spot of the drive laser. The x-rays and optical laser were then centred on the target.

X-ray diffraction data were collected by an array of CSPAD Detectors arranged in a transmission Debye-Scherrer geometry [18]. The 2D diffraction patterns from the individual detectors were integrated azimuthally and combined to produce 1D diffraction profiles extending from $2\theta = 18$ to 101° . A Velocity Interferometer System for Any Reflector (VISAR) diagnostic was used to both quantify the spatial planarity of the shock across the region of the target upon which the x-rays were incident,

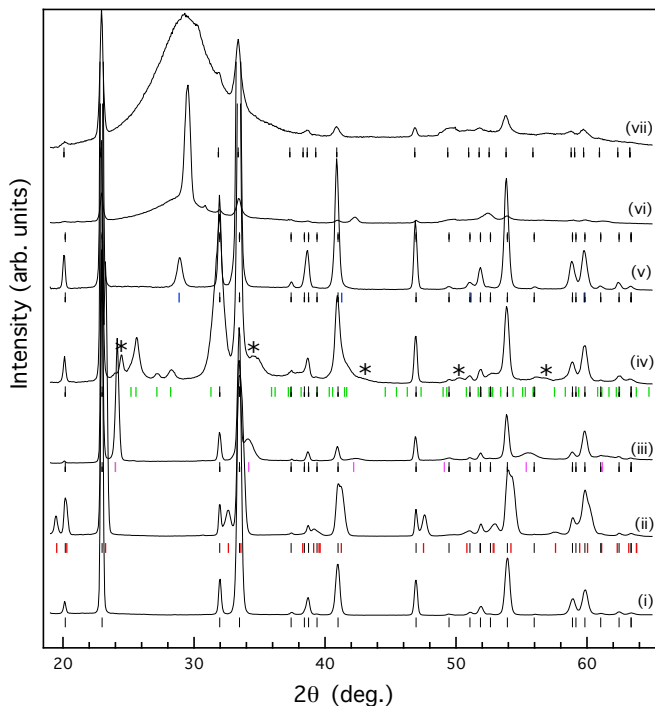


FIG. 1. Integrated profiles from shock-compressed Sb as a function of pressure. The colored tick marks beneath each profile show the calculated peak positions for the structures at those pressures while the black tickmarks beneath profiles (ii)-(vii) locate the peaks from the uncompressed Sb-I ahead of the shock front. The diffraction profiles are from (i) Sb-I (A7) at ambient pressure; (ii) compressed Sb-I at 1.9 GPa (red); (iii) Sb-I' fitted as simple cubic Sb without strength at 7.9 GPa (pink); (iv) Sb-II (HG) at 12.0 GPa (green); (v) Sb-III (bcc) at 18.9 GPa (blue); (vi) bcc/liquid Sb at 37.6 GPa; and (vii) liquid-Sb at 57.2 GPa. Asterisks in profile (iv) mark peaks from Sb-I'.

and measure the rear surface velocity of the Sb in order to determine the shock breakout time, and to calculate the pressure within the target via the Rankine-Hugoniot equations [15, 18, 25].

Unless explicitly stated, all x-ray data were collected on compression, that is, prior to the shock front reaching the rear surface of the Sb layer. Diffraction data were collected on compression, both with and without LiF windows, between 1.9 GPa and ~ 59 GPa. The as-grown Sb samples comprised longitudinally-oriented grains ~ 500 nm in diameter [18] and were highly textured, as revealed by the azimuthal variations in the intensity of D-S rings (see Figure S1). In marked contrast to the behaviour we observed previously in shocked Sc [15], sample texture persisted in both the compressed Sb-I and high-pressure phases. The sample was found, at ambient pressure, to have a fibre texture with the rhombohedral c -axis parallel to the sample normal; the texture was not characterised for the higher pressure phases.

Sb-I was seen on compression up to 6.9 GPa, with the Peierls distortion (as determined from the c/a axial ratio) reducing much more rapidly with pressure than has been reported previously in static compression studies [18]. On further compression to 7.9 GPa the diffraction pattern from the compressed sample simplified greatly, as shown in Figure 1, and could be fitted with a simple cubic structure. This un-distorted cubic structure is not obtained in the most recent static compression studies, but our results show that it can be created on nanosecond timescales via shock compression.

Although the spacing of the Sb-I' peaks indicated a cubic structure, profile (iii) in Figure 1 shows small but distinct displacements of several calculated peak positions from those observed in the integrated profile. Analysis of the 2D diffraction images revealed small azimuthal variations in the d-spacings of the D-S rings, suggesting the cubic phase exhibited some small degree of strength (i.e anisotropic strain) [18]. We quantified this using the methods described in [26], and this revealed that the distortion of D-S rings could indeed be explained by a cubic structure exhibiting strength [18].

However, the textured nature of the D-S rings, and the incomplete azimuthal coverage of the CSPAD detectors (see Figure S1), meant that a second structure, rhombohedral A7 with $u = \frac{1}{4}$ and c/a slightly less than $\sqrt{6}$, could not be excluded [18]. Had it been possible to collect the full 2D diffraction pattern then these two models would have been distinguishable [18]. Unfortunately, those areas of the 2D diffraction images where distinct differences in the diffraction patterns would be seen were not covered by the detectors.

On further compression above 11.3 GPa, the appearance of a completely different diffraction pattern signalled a transition to the Sb-II phase. While the D-S rings from this phase still exhibit azimuthal variations in intensity, they are undistorted and exhibit no detectable effects of

strain. Figure 2 shows a Rietveld fit to an almost single-phase diffraction pattern from incommensurate Sb-II obtained on release, 5 ns after the shockwave had entered the LiF window on the rear of the target. It is estimated that the subsequent release of the Sb sample to match impedance with the LiF would take ~ 4 ns. The pressure of the Sb sample immediately before arrival of the shock at the LiF interface was ~ 17 GPa, lowering to ~ 14 GPa after release. This indicates that the sample had released from the higher-pressure bcc phase (obtained above 14.6 GPa, see below), back into the HG phase. The refined parameters of the Sb-II structure, utilising superspace group $I'4/mcm(00\gamma)000s$, were $a_H = 7.983(3)$ Å, $c_H = 3.859(3)$ Å, and $\gamma = 1.305(5)$ ($V/V_0 = 0.767(1)$). The refined atomic coordinates for the host and guest atoms at the same pressure are $(0.153(1), x + \frac{1}{2}, 0)$ and $(0, 0, 0)$, respectively. These parameters are in excellent agreement with those obtained previously in a static compression study at 14.5 GPa and 300 K [27]. In contrast to the HG phase we observed in Sc under shock compression [15], the “guest-only” Bragg peaks that arise from scattering from only the guest atoms of the HG structure are clearly visible, as highlighted in Figure 2, showing that structures of the complexity of Sb-II can form completely in a nanosecond, with fully ordered incommensurate chains.

Further data collected late on free-surface release from targets without LiF windows also showed, in addition to

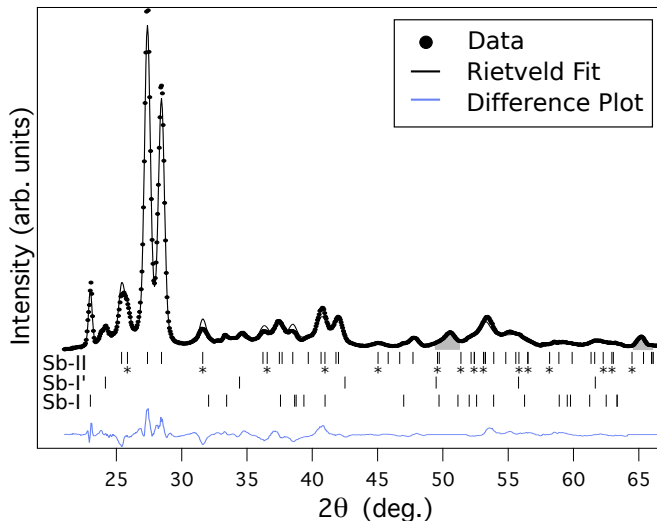


FIG. 2. A three phase (Sb-I, Sb-I', Sb-II) Rietveld fit to a diffraction profile of Sb obtained on release from ~ 17 GPa, for a Sb/LiF sample ($R_p=6.0\%$, $wR_p=6.7\%$, $\text{GoF}=1.12$ and $R(F^2)=3.4\%$ - see table S1). The calculated peak positions for Sb-I, Sb-I' (fitted as simple cubic) and Sb-II are shown by markers below the profile. The guest peaks from the HG phase, identified by starred tickmarks, confirm the guest chains are ordered. The grey shaded areas show two additional, unidentified peaks omitted from the three-phase fit.

Sb-I, diffraction peaks from the HG phase, with lattice parameters $a_H = 8.295$ Å, $c_H = 4.007$ Å, and $\gamma = 1.308$ ($V/V_0 = 0.860(3)$), slightly smaller than the values expected at ambient pressure [11, 12]. However, the same lattice parameters were obtained from data collected 6, 8, and 10 ns after initiation of release, providing evidence that the HG phase was at ambient pressure in each case. The HG phase was not observed in data collected more than 14 ns after release, placing an upper time limit on its stability at ambient pressure. This is the first time that a high-pressure incommensurate phase has been recovered to ambient pressure, and highlights the opportunities for transiently recovering exotic high-density phases to ambient conditions [28].

On increasing the drive pressure further, we observed a transition to the high-pressure bcc Sb-III phase at 14.6 GPa, much lower than the static compression transition pressure of 28.8 GPa at 300 K [27], and 20 GPa at the on-Hugoniot temperature of ~ 900 K [13] (Figure 4). At 37.6 GPa diffraction from liquid-Sb was first observed. The relative weakness of the liquid scattering compared to that from bcc (profile (vi) in Figure 1) suggests that melting had just initiated at this pressure. The bcc and liquid phases were found to co-exist between 37.6 and 59.2 GPa, where the sample has almost completely melted (profile (vii) in Figure 1). The Hugoniot and melting curve are therefore coincident over this pressure range.

Figure 4 shows, for comparison, a series of Hugoniot points from a previous gas gun study [5]. These data, along with subsequent published data sets, are included in our PT-Hugoniot calculations (as discussed in the supplementary material [18]). Differences between the two calculated PT-Hugoniots shown in Figure 4 arise from differences in thermodynamic variables used in the temperature calculations.

The observation of the Sb-I' phase, the transition pressure of 11.3 GPa to the HG phase, and the transition pressure of only 14.6 GPa to the bcc phase, are all strikingly different to the behaviour seen in static-compression studies of Sb at 300 K. In such studies the Sb-I' phase is not observed, and the transitions to the HG and bcc phases occur at 8.6 and 28.8 GPa, respectively [9, 27]. As our shock compression data were collected on the Hugoniot at elevated temperatures, it is possible that these different transition pressures arise simply from the different temperature regimes of the studies. However, we have recently conducted a high-temperature static compression study of Sb to 31 GPa and 835 K [13], the measured and extrapolated phase boundaries from which are shown in Figure 4. It is evident that the different behaviours seen in Sb under shock and static compression cannot be explained simply by the temperature differences, but must arise from the compression method. There is no evidence of the Sb-I' phase on static compression, and the shock-induced transition to Sb-I' occurs at a very similar pressure to the Sb-I \rightarrow Sb-II transition observed under static

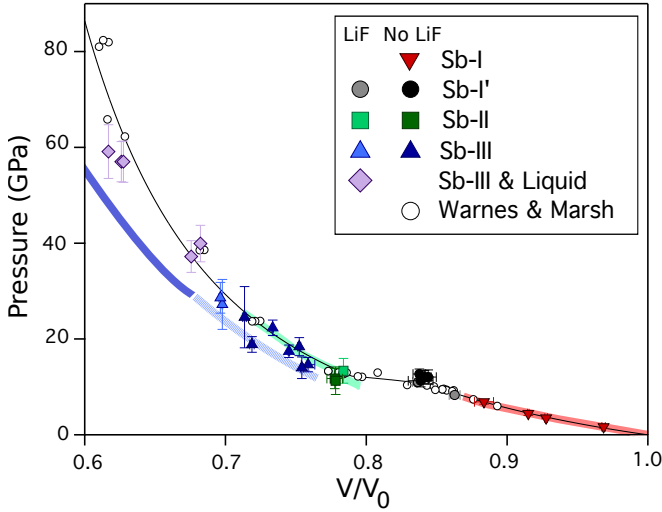


FIG. 3. The volumetric compression of Sb. Hugoniot EOS data obtained in this study are shown using coloured symbols, and points obtained using a LiF backing window are shown using lighter shaded symbols. The unfilled symbols show the previous shock compression data collected by Warnes and Marsh [3, 29]. The solid line through the data is calculated using two linear shock velocity (U_s) and particle velocity (u_p) relations ($U_s = 1.36u_p + 2.50$ below 10.6 GPa and $U_s = 1.65u_p + 1.93$ above 12.3 GPa), as detailed in the supplementary material [18]. The blue, green and red shaded lines show the isothermal compression of Sb-III, Sb-II and Sb-I, respectively, at 300 K [27]. The compressibility of Sb-III has been extrapolated below 28.8 GPa (shown as a lighter line) using a third-order Birch-Murnaghan EOS with $K' = 4$.

compression. This suggests that Sb-I' is a metastable extension of the Sb-I phase, accessed only via dynamic compression on the nanosecond timescales.

The calculations of Wang *et al* have highlighted the existence of transitions from the “normal” rhombohedral A7 structure to other A7 variants in the vicinity of the Sb-I \rightarrow Sb-II transition [32]. Specifically, they reported structural instabilities at 5.7 and 6.6 GPa to variants whose energy difference was so small (≤ 2 meV/cell) that the 5.7 - 6.6 GPa pressure range should be considered as a region of coexistence. While these A7 variants were not seen in our recent static compression study [13], Wang *et al* stated that transitions to them could be induced by the presence of a substantial uniaxial stress component along the c axis. As the microstructure of our deposited Sb layers comprises columnar grains (Figure S5), whose c -axes are aligned perpendicular to the layer, the crystallites are therefore compressed along their c -axes by the shock-wave, providing the uniaxial stress component considered by Wang *et al*. It is noticeable that the diffraction patterns from Sb-I' are the only ones exhibiting the distorted D-S rings that indicate a non-hydrostatic stress state. Further study would be required to confirm whether the Sb-I' phase is also observed under dynamic compression in samples exhibiting a different crystal orientation.

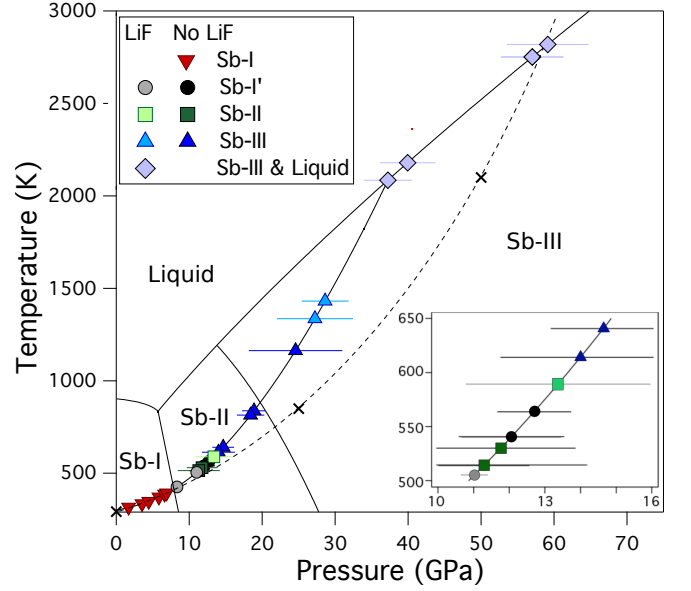


FIG. 4. The equilibrium phase diagram of Sb [13], along with the phases observed on compression in this study along the estimated Hugoniot [18]. The melting curve is given by a Simon-Glatzel fit to previously-observed melting curve data [30, 31] and the first LCLS data point in which liquid diffraction is observed. All other data points obtained from partially-melted samples are plotted on this estimated melt curve. Black crosses indicate Hugoniot points calculated in a previous gas-gun study, with a dashed line included as a guide to the eye [5].

The observation of the transition to the bcc Sb-III phase at only 14.6 GPa is very surprising, given the transition pressure of ~ 23 GPa seen in static compression studies at 650 K [13], and the transition pressure of 26.8 GPa determined from electronic structure calculations [12]. While transition pressures are often increased (overdriven) under dynamic compression [1] due to kinetic hinderance, the degree of *under-driving* we see in Sb is unusual, particularly as diffraction enables us to establish that the transition is to the same Sb-III structure seen in other studies. Our data suggest that transitions to cubic phases are favoured in Sb under dynamic pressure loading; this is a behaviour that has recently been reported in shock-compressed Bi [33], further study is needed to investigate whether this is also true for other materials that form complex structures under static compression.

Finally, we return to the identity of the ‘slow’ shock-induced phase transition reported previously above 8.8 GPa, with a volume change consistent with that found here for the Sb-I' \rightarrow Sb-II phase transition [1, 2]. The reported transition pressure sits squarely within the stability field established for Sb-I', and the reported transition time of 2-3 μ s is two orders of magnitude longer than our experimental timescales. However, the strong variation of transition pressure with sample thickness [3] suggests

that the transition pressure in our 10 μm thick samples would be much closer to the observed Sb-I' \rightarrow Sb-II transition pressure of 11.3 GPa. We would also expect to observe the transition on a much shorter timescale in our experiment: studies of the α - ϵ phase transition in iron have reported that shock stress and target thickness can cause significant variation in transition time [34, 35]. The two wave structure we see at ~ 12 GPa (as shown in Figure S3) is similar to that observed by Warnes [3] in conjunction with a phase transition, and is observed here in all samples where both Sb-I' and Sb-II are present in the diffraction patterns on compression. This enables us to establish that the previously observed transition, where the large volume reduction results in two-wave compression, arises from the Sb-I' \rightarrow Sb-II transition, with a transition time decreasing from microsecond to nanosecond timescales for increasing applied stress.

In conclusion, using x-ray diffraction at an XFEL we have been able to successfully observe and resolve the phase behaviour of shock-compressed Sb up to 59 GPa. We see a transition to Sb-I' at 7.9 GPa, a phase not seen in previous studies but which calculations suggest might arise as a result of uniaxial compression. This phase appears where the Sb-II host-guest structure forms under equilibrium conditions [13], as shown in Figure 4. A transition to Sb-II, with ordered guest chains, is found to occur on nanosecond timescales at 11.3 GPa, more than 3 GPa higher than in static compression studies, and this phase can be recovered to ambient pressure, where it is metastable for more than 10 ns. Sb-II is found to be stable to only 13.9 GPa, above which the cubic Sb-III phase is observed, ~ 8 GPa lower than its expected equilibrium transformation pressure of 23 GPa [13]. Sb-III remains the stable solid phase to 59 GPa, with melting beginning above 37.6 GPa.

Formation of the incommensurate Sb-II phase is thus strongly impeded on compression, with a new metastable phase (Sb-I') forming in its place, and the back transformation is impeded on release. There is also an anomalous under-driving of the transition to the higher-pressure Sb-III phase, at conditions where Sb-II is expected at equilibrium. This suggests a large kinetic barrier exists between the incommensurate host-guest structure and the structures of Sb-I, Sb-I', and Sb-III, all of which are cubic or slight distortions thereof, leading to the formation of metastable states. The resulting under-driving of a high-pressure transition stands in contrast to the expectation that kinetic effects only cause over-driving of phase transformations under dynamic compression [1]. Thus at most pressures where Sb-II is stable under equilibrium conditions, we observe other phases that are energetically less favourable, but which are more structurally accessible from the initial rhombohedral phase.

Our results clearly highlight both the differences in material properties which may arise as a consequence of compression technique and subsequent strain rates,

and the consequent importance of examining the detailed dynamic phase-transformation behaviour, which in this case differs considerably to that expected from studies at near-equilibrium conditions. Sb shows marked differences in structural behaviour between static and shock compression, especially in the dramatic contraction of the stability region of Sb-II in the latter, making the establishment of a universal phase diagram for Sb challenging. Study of these phase transitions using pressure loading mechanisms with intermediate characteristic sample strain rates (such as dynamic-DAC [36] or ramp-compression [37]) may elucidate how the kinetic and energetic transformation landscape evolves between equilibrium and ultrafast compression.

British Crown Owned Copyright 2018/AWE. Published with permission of the Controller of Her Britannic Majesty's Stationery Office. M.I.M. and J.S.W. would like to acknowledge support from EPSRC under Grant No. EP/J017256/1 and EP/J017051/1. D.M. is grateful to A.W.E for support. The work by J.H.E., D.E.F., R.F.S., D.C.S., and G.W.C. was performed under the auspices of the U.S. Department of Energy by Lawrence Livermore National Laboratory under Contract DE-AC52-07NA27344. C.A.B. would like to acknowledge support from Science Campaign 2 at Los Alamos National Laboratory, which is operated for the National Nuclear Security Administration of the U.S. Department of Energy under contract DE-AC52-06NA25396. Use of the Linac Coherent Light Source (LCLS), SLAC National Accelerator Laboratory, is supported by the U.S. Department of Energy, Office of Science, Office of Basic Energy Sciences under contract No. DE-AC02-76SF00515. The MEC instrument is supported by the U.S. Department of Energy, Office of Science, Office of Fusion Energy Sciences under Contract No. SF00515. We would like to thank Carol A. Davis and Paul Mirkirimi of LLNL for their help in preparing the Sb targets. Also we would like to thank Zeiss for their assistance in imaging the surface of the Sb samples. Finally, we extend our sincere thanks to the referees for their many useful comments and guidance.

-
- [1] G. E. Duvall and R. A. Graham, *Reviews of Modern Physics* **49**, 523 (1977)
 - [2] B. R. Breed and D. Venable, *Journal of Applied Physics* **39**, 3222 (1968)
 - [3] R. H. Warnes, *Journal of Applied Physics* **38**, 4629 (1967)
 - [4] R. E. Duff and F. S. Minshall, *Physical Review* **108**, 1207 (1957)
 - [5] R. G. McQueen and S. P. Marsh, *Journal of Applied Physics* **31**, 1253 (1960)
 - [6] L. F. Vereschagin and S. S. Kabalkina, *Sov Phys JETP* **20**, 274 (1965)
 - [7] T. N. Kolobyanina, S. S. Kabalkina, L. F. Vereschagin,

- and L. V. Fedina, Sov Phys JETP **28**, 88 (1969)
- [8] S. S. Kabalkina, T. N. Kolobyanina, and L. F. Vereschagin, Sov Phys JETP **31**, 259 (1970)
- [9] D. Schiferl, Review of Scientific Instruments **48**, 24 (1977)
- [10] H. Iwasaki and T. Kikegawa, Physica B & C **139**, 259 (1986)
- [11] O. Degtyareva, M. I. McMahon, and R. J. Nelmes, Physical Review B **70**, 184119 (2004)
- [12] U. Häussermann, K. Söderberg, and R. Norrestam, Journal of the American Chemical Society **124**, 15359 (2002)
- [13] A. L. Coleman, M. Stevenson, M. I. McMahon, and S. G. Macleod, Physical Review B **97**, 144107 (2018)
- [14] M. G. Gorman, R. Briggs, E. E. McBride, A. Higginbotham, B. Arnold, J. H. Eggert, D. E. Fratanduono, E. Galtier, A. E. Lazicki, H. J. Lee, H. P. Liermann, B. Nagler, A. Rothkirch, R. F. Smith, D. C. Swift, G. W. Collins, J. S. Wark, and M. I. McMahon, Physical Review Letters **115**, 095701 (2015)
- [15] R. Briggs, M. G. Gorman, A. L. Coleman, R. S. McWilliams, E. E. McBride, D. McGonegle, J. S. Wark, L. Peacock, S. Rothman, S. G. Macleod, C. A. Bolme, A. E. Gleason, G. W. Collins, J. H. Eggert, D. E. Fratanduono, R. F. Smith, E. Galtier, E. Granados, H. J. Lee, B. Nagler, I. Nam, Z. Xing, and M. I. McMahon, Physical Review Letters **118**, 025501 (2017)
- [16] B. Nagler, B. Arnold, G. Bouchard, R. F. Boyce, R. M. Boyce, A. Callen, M. Campell, R. Curiel, E. Galtier, J. Garofoli, E. Granados, J. Hastings, G. Hays, P. Heimann, R. W. Lee, D. Milathianaki, L. Plummer, A. Schropp, A. Wallace, M. Welch, W. White, Z. Xing, J. Yin, J. Young, U. Zastrau, and H. J. Lee, J. Synchrotron Rad **22**, 520 (2015)
- [17] D. C. Swift and R. G. Kraus, Physical Review E **77**, 066402 (2008)
- [18] See Supplemental Material <http://link.aps.org/supplemental/????> for additional information on the experimental procedure, the pressure determination, the Hugoniot model, the texture of the samples, the Sb-I' structural models and comparison with static data. which includes Refs. [18 - 24].
- [19] P. Hart, S. Boutet, G. Carini, M. Dubrovin, B. Duda, D. Fritz, G. Haller, R. Herbst, S. Herrmann, C. Kenney, et al., Proc. SPIE **8504**, 85040C (2012).
- [20] A. E. Gleason, C. A. Bolme, H. J. Lee, B. Nagler, E. Galtier, D. Milathianaki, J. Hawreliak, R. G. Kraus, J. H. Eggert, D. E. Fratanduono, G. W. Collins, R. Sandberg, W. Yang, and W. L. Mao, Nature Communications **6**, 8191 (2015)
- [21] “Antimony (sb) debye temperature, heat capacity, density, melting point: Datasheet from landolt-börnstein - group iii condensed matter · volume 41c: “non-tetrahedrally bonded elements and binary compounds i” in springer materials (https://dx.doi.org/10.1007/10681727_1148),” Copyright 1998 Springer-Verlag Berlin Heidelberg
- [22] G. V. Bunton and S. Weintroub, Journal of Physics C: Solid State Physics **2**, 116 (1969)
- [23] D. McGonegle, D. Milathianaki, B. A. Remington, J. S. Wark, and A. Higginbotham, Journal of Applied Physics **118**, 065902 (2015)
- [24] J. M. Brown and R. G. McQueen, Journal of Geophysical Research **91**, 7485 (1986)
- [25] P. M. Celliers, D. K. Bradley, G. W. Collins, D. G. Hicks, T. R. Boehly, and W. J. Armstrong, Review of Scientific Instruments **75**, 4916 (2004)
- [26] A. Higginbotham and D. McGonegle, Journal of Applied Physics **115**, 174906 (2014)
- [27] O. Degtyareva, M. I. McMahon, and R. J. Nelmes, High Pressure Research **24**, 319 (2004)
- [28] J. Sun, D. D. Klug, and R. Martoňák, The Journal of Chemical Physics **130**, 194512 (2009)
- [29] S. P. Marsh, *LASL Shock Hugoniot data. Los Alamos series on dynamic material properties* (University of California, 1980)
- [30] S. M. Stishov and N. A. Tikhomirova, Sov Phys JETP **48**, 1215 (1965)
- [31] W. Klement, A. Jayaraman, and G. C. Kennedy, Physical Review **131**, 632 (1963)
- [32] X. Wang, K. Kunc, I. Loa, U. Schwarz, and K. Syassen, Physical Review B **74**, 134305 (2006)
- [33] M. G. Gorman, A. L. Coleman, R. Briggs, R. S. McWilliams, D. McGonegle, C. A. Bolme, A. E. Gleason, E. Galtier, H. J. Lee, E. Granados, M. a. x. liwa, C. Saneloup, S. Rothman, D. E. Fratanduono, R. F. Smith, G. W. Collins, J. H. Eggert, J. S. Wark, and M. I. McMahon, Nature Publishing Group , 1 (2018)
- [34] B. J. Jensen, G. T. Gray III, and R. S. Hixson, Journal of Applied Physics **105**, 103502 (2009)
- [35] R. F. Smith, J. H. Eggert, D. C. Swift, J. Wang, T. S. Duffy, D. G. Braun, R. E. Rudd, D. B. Reisman, J. P. Davis, M. D. Knudson, and G. W. Collins, Journal of Applied Physics **114**, 223507 (2013)
- [36] Z. Konôpková, A. Rothkirch, A. K. Singh, S. Speziale, and H.-P. Liermann, Physical Review B **91**, 144101 (2015)
- [37] A. Lazicki, J. R. Rygg, F. Coppari, R. Smith, D. Fratanduono, R. G. Kraus, G. W. Collins, R. Briggs, D. G. Braun, D. C. Swift, and J. H. Eggert, Physical Review Letters **115**, 075502 (2015)